Bol. Soc. Esp. Mat. Apl.
nº 48(2009), 29–55

TRACKING FLUID INTERFACES APPROACHING SINGULAR EVENTS

HECTOR D. CENICEROS

Department of Mathematics
University of California, Santa Barbara

hdc@math.ucsb.edu

Abstract

The motion of fluid interfaces often lead to singular events which include pinching, break-up, coalescence, and cusp formation. Numerical simulation can play a key role in the investigation of these fundamental phenomena which is of significant scientific and technological interest. This is however a formidable task which demands an accurate resolution of disparate time and length scales and a faithful representation of physical forces. A survey of front-tracking methods for the investigation of singular or near singular events in interfacial rheology is presented. This review is focused on immersed interface and boundary integral type methods. Recent advances and some salient remaining challenges are also discussed.

Key words: *Front-tracking methods, break-up, coalescence, topological singularities, multi-phase flows, surface tension*

AMS subject classifications: *65N38 76B07 76B45 76B70 76D07 76D27*

1 Introduction

The dynamics of fluid interfaces that bound drops, bubbles, jets, or layers of fluids with different material properties is a source of intriguing and fascinating singular and small-scale phenomena which include pinching, break-up, coalescence, cusp formation, short capillary waves, and many of the fundamental instabilities in fluids. These examples have inspired, over the course of several decades, the development of many numerical approaches to follow the motion of these free boundaries for a variety of flows. The methods are broadly divided into two main types: *front-tracking and front-capturing*. In a front-tracking method [58, 82, 36, 34, 35, 48], the fluid interface is evolved in time by updating an explicit representation of the interface in the form of links, elements, or Lagrangian markers. In contrast, in a front-capturing approach the interface is embedded as a level set of a function defined in the

Fecha de recepción: 19/03/2009. Aceptado (en forma revisada): 07/06/2009.

entire fluid (computational) domain. This function could be an approximation to the distance to the interface (level set method [57, 24, 76]), a volume fraction of one of the two component in a two-phase flow (Volume-Of-Fluid method [69, 63, 66, 60]), or a concentration-related order parameter (phase field method [25, 3, 45, 13, 6, 46, 88]).

Despite significant advances, both approaches, tracking and capturing, have shortcomings when it comes to dealing with topological singularities. In tracking, a decision has to be made to allow or not a topological transition (e.g. break-up, merging) and if so when and how an interfacial reconnection is to be performed. The process remains unsatisfactorily manual and different procedures can lead to dramatically different outcomes (see for example [56]). On the other hand, in a front-capturing method, the transition through a topological singularity occurs without user intervention. While this can be advantageous for some applications that do not require small-scale details of the flow, it is a serious drawback for the investigation of the interfacial rheology immediately preceding a singular or near singular event. The realization of such singular phenomena is very much flow-dependent. Real fluid interfaces can remain in extreme close proximity for some time without reconnecting. Unfortunately, a front-capturing method typically precipitates a topological change under such conditions. Moreover, interacting fluid interfaces frequently develop small-scale structure in the form of localized curvature variations, and short, capillary waves which are difficult to resolve with a front-capturing approach. Thus, despite post-singularity limitations, front-tracking methods appear to be more suitable for the investigation of the interfacial rheology leading to a potential topological singularity.

In this article, we review two classes of tracking methods for the investigation of a potentially singular events in an interfacial flow. The methods considered are based on the boundary integral approach and the immersed boundary method. The presentation and discussion are focused on 2D flows. We present an illustrative example of flow-induced drop coalescence and a case Rayleigh-Taylor instability for both inviscid and viscous flows.

2 Boundary integral methods

Boundary integral methods are a powerful numerical tool for a specialized class of problems. These methods have been used extensively to study the motion of single or multiple drops or bubbles in Stokes flows (see e.g. the reviews [1, 2] and [74, 52, 49, 91, 26, 28]). The boundary integral approach is attractive because it reduces the problem to one defined on the interface only. Thus, it provides a framework within which it is possible to achieve, at least in principle, high resolution of interfacial quantities, which is necessary for the investigation of the small scale phenomena that occur during the fundamental processes of coalescence and break-up.

In what follows we are going to assume that we have a fluid interface or immersed boundary Γ represented in parametric form at time t as $\mathbf{X}(\alpha, t)$ for

$\alpha \in B$. Here α is a Lagrangian parameter, not necessarily arclength, and $B \subset \mathbb{R}$.

2.1 Inviscid flows

The first example we consider is a density-stratified fluid. The system consists of two infinite layers of fluid which are inviscid, incompressible, and irrotational. A fluid interface Γ separates the layers. We denote the fluid quantities above the interface with the subscript 2 and those below the interface with subscript 1. The fluid in each layer satisfies Euler's equations

$$\rho_i \left(\frac{\partial \mathbf{u}_i}{\partial t} + \mathbf{u}_i \cdot \nabla \mathbf{u}_i \right) = -\nabla p_i - \rho_i \mathbf{g} \tag{1}$$

$$\nabla \cdot \mathbf{u}_i = 0, \tag{2}$$

for $i = 1, 2$, where ρ_i, $\mathbf{u}_i$, and p are the density, velocity, and pressure respectively. The constant force $\mathbf{g}$ represents the gravity acceleration. Due to the assumption of irrotationality, we have that in the bulk fluid

$$\nabla \times \mathbf{u}_i = 0, \qquad i = 1, 2. \tag{3}$$

Two boundary conditions are imposed on Γ. A kinematic boundary condition which states that the normal velocity is continuous across Γ and a dynamic boundary condition which takes the form of the so-called Laplace-Young law

$$[p]_\Gamma = \tau \kappa, \tag{4}$$

where $[p]_\Gamma$ denotes the jump of pressure across the interface Γ, κ is the mean curvature, and τ is the surface tension coefficient. Note that, in consistency with the kinematic boundary condition, the tangential velocity at the fluid interface is not uniquely determined as it may have a jump discontinuity across Γ.

In two dimensions, it is convenient to work with a complex position variable $z(\alpha, t) = x(\alpha, t) + iy(\alpha, t)$ where x and y are the two components of $\mathbf{X}(\alpha, t)$. Closed (periodic) interfaces and open but periodically extended interfaces in the horizontal direction are commonly used configurations. For the latter we have $z(\alpha, t) = \alpha + p(\alpha, t)$, where $p(\alpha, t)$ is a 2π-periodic function of α.

Taking the tangential velocity to be the average of the limiting velocities above and below the interface, the interface evolves according to the Birkhoff-Rott equation

$$\frac{d\bar{z}}{dt}(\alpha, t) = \frac{1}{4\pi i} \int_{-\pi}^{\pi} \gamma(\alpha', t) \cot \frac{1}{2}(z(\alpha, t) - z(\alpha', t)) d\alpha', \tag{5}$$

where the periodicity has been employed to obtain a closed form of the kernel. In (5) $\bar{z}$ is the complex conjugate of z and γ is the unnormalized vortex sheet strength. The above integral should be understood as the Cauchy principal-value integral. If the interface is closed, then $z(\alpha, t)$ is a periodic function of α the the Birkhoff-Rott equation becomes

$$\frac{d\bar{z}}{dt}(\alpha, t) = \frac{1}{2\pi i} \int_{-\pi}^{\pi} \frac{\gamma(\alpha', t)}{z(\alpha, t) - z(\alpha', t)} d\alpha'. \tag{6}$$

Using Euler's equations (1) on both sides of Γ we can obtain an evolution equation for this vortex sheet strength in the form [8]:

$$\frac{d\gamma}{dt} = -2A\left(Re\left\{\frac{d^2\bar{z}}{dt^2}z_\alpha\right\} + \frac{1}{8}\partial_\alpha\left(\frac{\gamma^2}{|z_\alpha|^2}\right) + gy_\alpha\right) + S\kappa_\alpha, \tag{7}$$

where $A = (\rho_1 - \rho_2)/(\rho_1 + \rho_2)$ is the Atwood number and $S = \tau/(\rho_1 + \rho_2)$ is a scaled surface tension parameter. Due to the first term in the right hand side of (7), this is a Fredholm integral equation of the second kind for $d\gamma/dt$. It can be shown that this equation has a globally convergent Neumann series [8] and as a result, it can be solved efficiently via fixed point iteration. Of course, if $A = 0$ (density matched case) then $d\gamma/dt$ is given explicitly; this is the classical, inertial vortex sheet case. Equations (5) and (7) completely determine the motion of the free boundary.

2.1.1 Numerical methods

The design of numerical methods for (5) or (6) and (7) appears deceivable simple; just specify a quadrature Q_h to evaluate the integral in (5), an approximation D_h to the derivative ∂_α, and a time stepping scheme. Unfortunately, boundary integral methods for inviscid flows are notoriously sensitive to numerical instabilities [50, 67, 30]. This problem is excerbarated by the presence of surface tension as it contributes with nonlinear terms with high order derivatives. In the case of 2D water waves, Beale, Hou, and Lowengrub [10] showed that a delicate balance of leading order singular operators that exists at the continuum level must be retained at the discrete level to achieve numerical stability. As a consequence, Q_h and D_h cannot be chosen independently. The stability analysis in [10] was subsequently extended to the more general case of two-fluid interfaces with surface tension in [16].

The presence of surface tension also induces a time-step constraint to explicit time integration schemes of the form

$$\Delta t < \frac{C}{S}(\min_i \Delta s_i)^{3/2}, \tag{8}$$

where $\Delta s_i = |z_\alpha| h$ is the spacing between Lagrangian markers, $h = 2\pi/N$, and N is the total number of markers or interfacial points. This constraint is typically a severe one due to excessive clustering of Lagrangian points as these are advected by the flow. The numerical stiffness introduced by surface tension was a serious limitation to long time simulations of interfacial flows in 2D via boundary integral techniques. An efficient approach that overcame this difficulty was proposed by Hou, Lowengrub, and Shelley [41]. The central idea of their method is to employ more convenient variables to describe the interface position, namely the tangent angle θ and the arclength metric $\sigma = |z_\alpha|$, to extract leading order terms at small scales (high wave numbers), and to treat the latter implicitly. Indeed, in terms of θ and σ, we have that the curvature has the simple form $\kappa = \frac{1}{|z_\alpha|}\theta_\alpha$. Henceforth, we denote with the subscript α

differentiation with respect to that variable. This expression for the curvature can be further simplified by selecting a parametrization or frame that produces a spatially independent arclength metric $|z_\alpha|$, i.e. one in which the Lagrangian particles remain equidistributed in arclength. Such a dynamic parametrization change can be achieved by exploiting the freedom in specifying the tangential velocity [41].

Let $W = \frac{d\bar{z}}{dt}$, then we can write the flow's normal and tangential components of the velocity at Γ as $U^N = -Im\{e^{i\theta}W\}$ and $U^T = Re\{e^{i\theta}W\}$ with Re and Im denoting the real and imaginary parts respectively. The boundary integral representation (5) and (7) can be reformulated in the new frame and variables as

$$\sigma_t = \left(U^T + U^A\right)_\alpha - \theta_\alpha U^N. \tag{9}$$

$$\theta_t = \frac{1}{\sigma}\left[U^N_\alpha + \theta_\alpha(U^T + U^A)\right], \tag{10}$$

$$\begin{aligned}\gamma_t = {} & S\left(\frac{\theta_\alpha}{\sigma}\right)_\alpha + \left(\frac{\gamma}{\sigma}U^A\right)_\alpha \\ & - 2A\left[Re\{\sigma e^{i\theta}W_t\} + \frac{1}{8}\left(\frac{\gamma}{\sigma}\right)^2_\alpha + g\sigma\sin\theta - U^A Re\{e^{i\theta}W_\alpha\}\right],\end{aligned} \tag{11}$$

where U^A is an added tangential velocity that can be used to control the spacing of Lagrangian particles. In particular, one could choose a U^A that renders a space-independent σ that is equal to its average at all times

$$\sigma(\alpha, t) = < \sigma >, \tag{12}$$

where $< \cdot >$ stands for the mean in α over one period. It is easy to show that if

$$U^A = -U^T + \int_0^\alpha \left[\theta_\alpha U^N - \left\langle \theta_\alpha U^N \right\rangle\right] d\alpha', \tag{13}$$

then the constraint (12) is enforced at all times provided it holds initially. With this choice of U^A, (9) becomes the ordinary differential equation

$$\sigma_t = -\left\langle \theta_\alpha U^N \right\rangle. \tag{14}$$

The leading order terms at small scales can be easily extracted from this formulation. Extending the periodic integrand in (5) to the entire real line we can write

$$W = \frac{1}{2\pi i}\int_{-\infty}^{\infty} \frac{\gamma(\alpha')}{z(\alpha) - z(\alpha')} d\alpha' = \frac{1}{2iz_\alpha}\mathcal{H}[\gamma] + \int_{-\infty}^{\infty} \gamma(\alpha') g(\alpha, \alpha') d\alpha', \tag{15}$$

where $\mathcal{H}$ is the Hilbert transform defined by

$$\mathcal{H}[f](\alpha) = \frac{1}{\pi}\int_{-\infty}^{\infty} \frac{f(\alpha')}{\alpha - \alpha'} d\alpha', \tag{16}$$

and g is a smooth function. Thus, it follows that

$$U^N(\alpha,t) = \frac{1}{2\sigma}\mathcal{H}[\gamma](\alpha,t) + R_s[\gamma](\alpha,t), \tag{17}$$

where R_s is a smoothing operator in the sense that if $z(\alpha,t)$ is a real analytic function of α for $t \leq T$ and $\sigma > 0$ then the Fourier transform of R, satisfies $\hat{R}_s[\gamma] = O(e^{-\rho|k|}\hat{\gamma})$ for large wavenumber $|k|$. Here, $\rho > 0$ is the width of the strip of analyticity about the real axis. If $z(\alpha,t)$ is only C^m then $\hat{R}_s[\gamma] = O(|k|^{-m}\hat{\gamma})$. Thus, at high modes,

$$\frac{1}{\sigma}U^N_\alpha \sim \frac{1}{2\sigma^2}\Lambda[\gamma],$$

where $\Lambda = \partial_\alpha \mathcal{H}$ and by $\sim$ we mean equivalent modulo a smoothing operator. The evolution equations for θ and γ can now be written in a form that reveals the leading order behavior at small scales:

$$\theta_t = \frac{1}{2\sigma^2}\Lambda[\gamma] + P, \tag{18}$$

$$\gamma_t = \frac{S}{\sigma}\theta_{\alpha\alpha} + Q, \tag{19}$$

where P is defined as the right hand side of (10) minus the high mode leading term and Q is the right hand side of (11) without the surface tension term. Note that both leading order terms in (18) and (19) are diagonal in Fourier space. Consequently, a semi-implicit discretization in which these two terms are treated implicitly while keeping P and Q explicitly produces a simple 2×2 linear system for each mode k. A forth order implicit/explicit SBDF method [4] has been used successfully in several applications [41, 42, 16, 17, 18, 23].

The leading order terms at small scales (high modes) balance each other out. Indeed, if we multiply (18) by $\Lambda[\theta]$ and (19) by $\gamma/(2S\sigma)$ and note that $\theta_{\alpha\alpha} = -\Lambda^2\theta$ we obtain

$$\frac{1}{2}\frac{d}{dt}\int \theta\Lambda[\theta]d\alpha = -\frac{1}{2\sigma^2}\int \Lambda[\theta]\Lambda[\gamma]d\alpha + \ldots \tag{20}$$

$$\frac{1}{4\sigma S}\frac{d}{dt}\int \gamma^2 d\alpha = -\frac{1}{2\sigma^2}\int \Lambda[\theta]\Lambda[\gamma]d\alpha + \ldots \tag{21}$$

To guarantee numerical stability it is crucial to maintain this type of balance among leading order terms at the discrete level. This balance and hence numerical stability can be achieved with a spectral spatial discretization and suitable de-aliasing filtering as proved in [16]. For both configurations, Γ closed or $z(\alpha,t) = \alpha + p(\alpha,t)$ with $p(\alpha,t)$ periodic, it is possible to obtain a spectral discretization in α of the evolution equations (9)-(11). The Birkhoff singular integral in (5) or in (6) can be computed with spectral accuracy via the alternate-point trapezoidal rule [71, 70]

$$W_i = \frac{1}{4\pi i}\sum_{\substack{j=-N/2+1 \\ (j-i)\ \text{odd}}}^{N/2} \gamma_j \cot\frac{1}{2}(z_i - z_j)2h, \tag{22}$$

where $h = 2\pi/N$, with N even. This quadrature results from Richardson extrapolation and cancels out the kernel's singularity. Derivatives with respect to α can be computed (pseudo) spectrally via the Fast Fourier Transform (FFT).

2.1.2 Potential pinch-off in unstably stratified 2D flows

One of the fundamental instabilities in incompressible fluids takes place at the interface of two fluids with different densities when the lighter fluid is accelerated into the heavier fluid [31]. This instability is called Rayleigh-Taylor (RT) [65, 77] and is believed to play a preeminent role in fluid mixing which is important to a wide variety of applications. Due to its fundamental relevance and applications, several numerical studies have been performed [27, 7, 64, 9, 78, 33, 39, 35, 84, 5, 40] and the RT instability has also served as a test case for numerical methods of multi-phase flows [38, 11, 63, 16, 60].

In the absence of any regularizing mechanism, an unstably stratified inviscid fluid system is linearly ill-posed due to the RT instability. Surface tension tension can provide a physically-based regularization to the RT instability and at the same time also be a driving force in nonlinear regimes. A number of experimental [83] and numerical studies [78, 11, 60, 16] of the RT instability have shown that for an interface that is initially a single-mode perturbation of a flat sheet (single-mode setup), at small to moderate Atwood numbers, the interface develops thin fluid fingers that subsequently roll-up and form a mushroom shaped configuration. However, in some of the numerical studies that show roll-up and eventual drop formation there is no surface tension and thus the regularizing mechanisms are purely numerical. Thus, to understand the critical effects of surface tension it is of paramount importance that these are captured accurately and are not overshadowed by numerically induced regularizations. This is particularly relevant near a potentially singular event such as pinch-off or drop formation. The spectrally accurate, non-stiff, boundary integral method described in 2.1.1 provides an effective tool for such an investigation in the case of inviscid flows.

As an illustration of the importance of surface tension effects on the long-time motion of an unstably stratified *inviscid* fluid we consider a case originally reported in [16] of an initial single mode perturbation

$$z(\alpha, 0) = \alpha + i\epsilon \cos(2\pi\alpha), \tag{23}$$

$$\gamma(\alpha, 0) = 0, \tag{24}$$

where $\epsilon = 0.1$ and we take $A = -0.1$, $g = 10$, and $S = 0.005$. Figure 1 shows the time evolution of the interface for a calculation employing $N = 1024$ and $\Delta t = 1.25 \times 10^{-4}$. Near $t = 0.8$, the interface becomes vertical in two symmetric positions about $x = 0.5$. Two small fluid fingers develop and subsequently roll up. A close-up look at the subsequent dynamics is presented in Fig. 2 where capillary waves emanating from the rolled up fingers could be clearly observed. Opposite to the finger tips of the heavier fluid, small bumps with high curvature develop and the two opposite sections of the interface approach

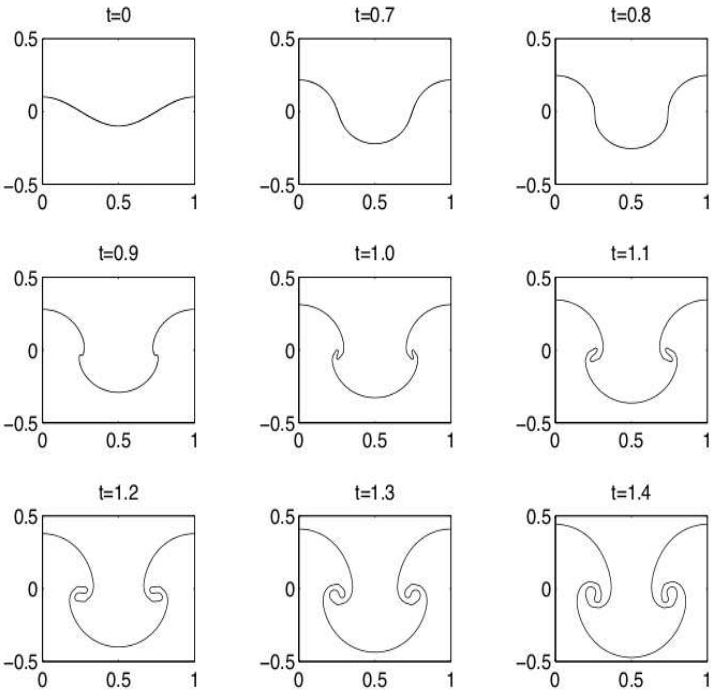

Figure 1: Unstably stratified inviscid flow: Time evolution of the interface with $A = -0.1$ and $S = 0.005$. $N = 1024$ and $\Delta t = 2.5 \times 10^{-4}$.

each other during roll-up. During this process a thin film ensues and the interfacial portions in close proximity develop large curvatures as the thin film drains. Figure 3a shows the interface profile at $t = 1.785$ and Fig. 3b displays the minimum interfacial separation or thin film thickness which continues to decrease in time. The monotone behavior of the thin film thickness is a strong indication of a finite-time topological singularity formation. A fit to a curve of the form $d(t) = C(t_c - t)^{2/3}$, shown as a solid line in Fig. 3b, shows good agreement with the numerical data. This suggests that the interface might collapse with a 2/3 exponent but a further numerical and analytical study is needed to have a more conclusive answer; this is still an open problem.

A remarkably similar topological singularity formation was also observed by Hou, Lowengrub, and Shelley [42] in their investigation of vortex sheet (density matched) undergoing Kelvin-Helmholtz instability in the presence of surface tension. The coinciding aspects of these two different problems, Kelvin-Helmholtz instability and RT instability, suggests that surface tension leads to and ultimately determines the type of interfacial collapse. This topological singularity is truly surprising as it is driven by surface tension and it takes place in a 2D flow where the azimuthal component of the curvature is absent.

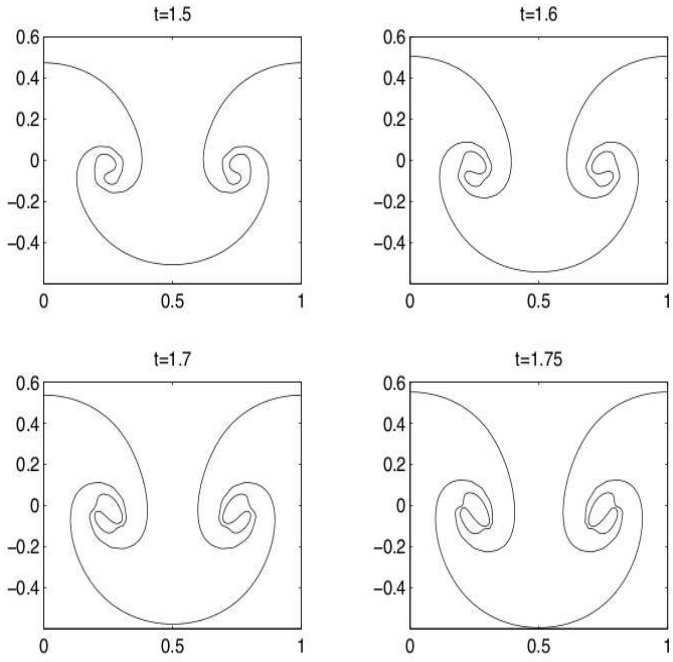

Figure 2: Unstably stratified inviscid flow: $A = -0.1$ and $S = 0.005$. Sequence of interface positions. $N = 2048$ and $\Delta t = 1.25 \times 10^{-4}$.

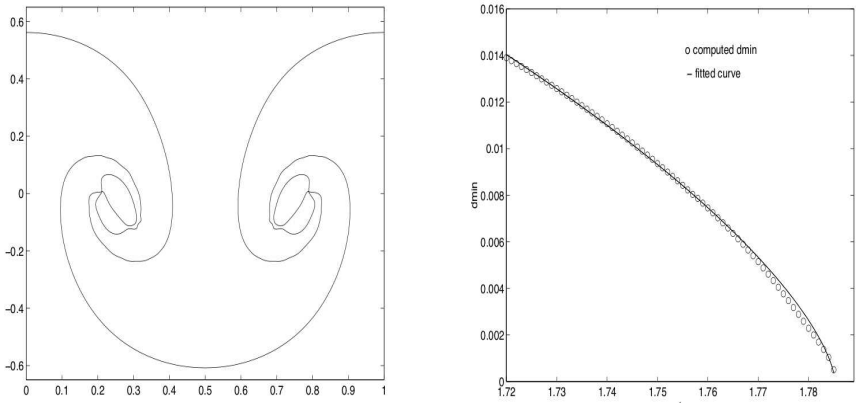

Figure 3: Unstably stratified inviscid flow: $A = -0.1$ and $S = 0.005$. (a) Interface position at $t = 1.785$ and (b) minimum separation against time. The circles represent the computed values and the solid line a fitted curve of the form $d(t) = C(t_c - t)^{2/3}$.

2.2 Stokes flows

The problem of flow-induced drop coalescence has received considerable recent attention due to the role that this process plays in the formation of polymer blends, which is currently the major route to new polymeric materials with desired macroscopic properties. The understanding of the conditions for coalescence and their dependence on fluid and flow properties is critical for controlling this process.

In coalescence experiments with drops whose diameters are $O(100)$ microns [47, 86], the Reynolds number Re, which is a relative measure of inertia versus viscous forces, is very small and inertia can neglected (Stokes flow). In such situations, a boundary integral representation of the interfacial velocity can be obtained in terms of the jump in the interfacial surface force. This representation, as a computational method, was first described by Youngren and Acrivos [87] and since then significant progress has been made in the extensions of the boundary integral formulation and on improvements of its accuracy as reviewed by Pozrikidis [61, 62].

Let us consider two drops of Newtonian fluid with viscosity μ_d surrounded by an unbounded Newtonian fluid of viscosity μ_e and affected by an external flow field $\mathbf{u}^\infty$. Neglecting inertia terms, the velocity components u_j on the drop surfaces S_1 and S_2 can be written in the following boundary integral representation (using the summation convention over repeated indices) [61] :

$$\begin{aligned} u_j(\mathbf{x_0}) = \frac{2}{1+\lambda} u_j^\infty(\mathbf{x_0}) - \frac{1}{4\pi\mu_e(1+\lambda)} \int_S G_{ij}(\mathbf{x},\mathbf{x_0})[f_i(\mathbf{x})]_S \, dS(\mathbf{x}) \\ + \left(\frac{1-\lambda}{1+\lambda}\right) \frac{1}{4\pi} \int_S u_i(\mathbf{x}) T_{ijk}(\mathbf{x},\mathbf{x_0}) n_k(\mathbf{x}) \, dS(\mathbf{x}), \end{aligned} \tag{25}$$

for $\mathbf{x_0} \in S$ and $j = 1, 2, 3$. Here $\lambda = \mu_d/\mu_e$, $S = S_1 + S_2$, n_k denotes the components of the (outward) unit normal, and $[f_i(\mathbf{x})]_S$ expresses the jump in the interfacial force. For example, in the case of uniform surface tension $[f_i(\mathbf{x})]_S = 2\tau\kappa n_i$, where τ is the surface tension coefficient and κ is the mean curvature, is the classical Laplace-Young formula. In (25), G_{ij} is the Stokeslet tensor (free space Green's function)

$$G_{ij}(\mathbf{x},\mathbf{x_0}) = \frac{\delta_{ij}}{\|\mathbf{x}-\mathbf{x_0}\|} + \frac{(x_i - x_{0i})(x_j - x_{0j})}{\|\mathbf{x}-\mathbf{x_0}\|^3}, \tag{26}$$

where δ_{ij} is the Kronecker delta. T_{ijk} is the associated stress tensor

$$T_{ijk}(\mathbf{x},\mathbf{x_0}) = -6\frac{(x_i - x_{0i})(x_j - x_{0j})(x_k - x_{0k})}{\|\mathbf{x}-\mathbf{x_0}\|^5}. \tag{27}$$

The integral involving G is known as the single-layer potential while that involving T is referred to as the double-layer potential. Given the interfacial force jump $[\mathbf{f}]_S$, (25) represents a Fredholm integral equation for the interfacial velocity. When the viscosity of the drop and the ambient fluid are matched the velocity is given solely by the single layer integral.

Due to the non-removable singular nature of the integrands in both the single-layer potential and the double-layer potential the design of quadratures with high order uniform accuracy is a challenging problem. The following two flow identities

$$\int_S G_{ij}(\mathbf{x}, \mathbf{x_0}) n_i(\mathbf{x}) dS(\mathbf{x}) = 0. \tag{28}$$

$$\int_S T_{ijk}(\mathbf{x}, \mathbf{x_0}) n_k(\mathbf{x}) dS(\mathbf{x}) = -4\pi\delta_{ij}, \tag{29}$$

for $\mathbf{x_0} \in S$, are often employed to ameliorate the singularities and to produce bounded integrands. However, it is important to note that higher order derivatives of the integrands remain singular. In addition, the evaluation of the integrals in three dimensions is a costly operation. While there has been some progress in the application of fast multipole techniques to expedite the computation of these boundary integrals [90], the level of resolution and high accuracy required in the 3D exploration of topological singularity events, such as coalescence and break-up, remains largely unattainable.

To reduce the computational complexity, often an assumption of axial symmetry is taken. With this axi-symmetric flow assumption an analytic integration around the axis of symmetry can be performed using cylindrical coordinates and the surface integrals in (25) reduce to line integrals over the curve C traced by the drops on a plane with fixed (zero) azimuthal angle (see e.g. [61]). The resulting kernels of these line integrals can be expressed in terms of complete elliptic integrals [61]. Using (28)-(29) and the trapezoidal rule it is possible to obtain second order quadratures for the line integrals. Recently, higher order quadratures with error corrections obtained from asymptotic expansions have been proposed in [19].

The components of the normal as well as the curvature can be evaluated with standard finite differences, with splines, or spectrally. To evolve the fluid interfaces (the trace C of the drops) we again have freedom in specifying the tangential velocity. Thus, we may write

$$\frac{\partial \mathbf{x}}{\partial t} = \mathbf{u} + U^A \mathbf{t}, \tag{30}$$

where $\mathbf{t}$ is a unit tangent vector. Equation (30) can be integrated with a high order Runge-Kutta method or a multi-step method.

The following example of flow-induced coalescence in axi-symmetric geometry illustrate some of the computational challenges to investigate this important singular phenomenon.

2.2.1 Drop coalescence

In a drop coalescence problem the interfacial region of interaction, which is expected to experience the largest deformation, is very much fixed or can be easily predicted. As a consequence, high resolution can be obtained adaptively

by specifying the additional tangential velocity U^A so that

$$\sigma(\alpha, t) = R(\alpha) < \sigma >, \tag{31}$$

where $R > 0$ is a smooth function of mean one. Naturally, R should be chosen to be small around the interaction region that requires high resolution. Examples of such a R have been presented in [41, 85].

In a Stokes flow approximation coalescence cannot occur in finite time due to lubrication forces unless long-range, van der Waals-type of forces, are taken into account. To a first approximation, these could be modeled by introducing a disruptive pressure into the interfacial force jump so that the surface tension force gets replaced by

$$[f_i(\mathbf{x})]_S = 2\tau\kappa n_i - \frac{A_H^*}{h(\mathbf{x})^3} n_i, \tag{32}$$

where A_H^* is a scaled Hamaker constant and $h(\mathbf{x})$ is the drop-drop separation distance (see e.g. [47]).

We present next results originally reported in [85] for a numerical investigation of flow-induced coalescence of two equal-sized drops in axi-symmetric flows. The simulation is performed with using the boundary integral formulation described in this section. Normal and tangent vectors, as well as the curvature are computed spectrally by periodic extension of the drop position variable $\mathbf{X}(\alpha, t)$. An adaptive Lagrangian mesh is obtained by employing a U^A to enforce (31) with a judiciously chosen R to accurately resolve localized, high curvature regions and integration of (30) is performed with a second order Runge-Kutta scheme. The flow is characterized by a capillary number $Ca = \mu_e G R/\tau$, where G is the strain rate of the imposed, steady, bi-axial flow $\mathbf{u}^\infty$ (to simulate head-on collisions), and R is the radius of the undeformed drops. The viscosity ratio is $\lambda = 0.19$, $R = 27.2\mu m$, and $A_H^* = 4.99 \times 10^{-11}$.

Figure 4 compares the center-to-center distance d of the drop as a function of the dimensionless time tG for an experiment with that obtained from the boundary integral simulations for $Ca = 0.0207$. The insets display the computed drop profile at $t = 0.815$ when $d = 2R$ and at $tG = 2.041$. The numerical simulation predicts very well the drainage time of the thin film separating the two drops as well as their deformation. Moreover, with the numerics we can look at the interfacial deformation in the neighborhood of the contact region (thin film shape). Such an observation is impossible in the experiments. Figure 5 presents a close-up of the thin film change as it evolves dynamically. The fluid interfaces experience a large deformation at the impending collapse. High resolution is essential for capturing this singular event.

3 Immersed boundary-type methods

Fluid interfaces that bound drops, bubbles, and layers composing multi-phase systems can be viewed as immersed structures or boundaries interacting with the flow. There is a myriad of technologically and scientifically important

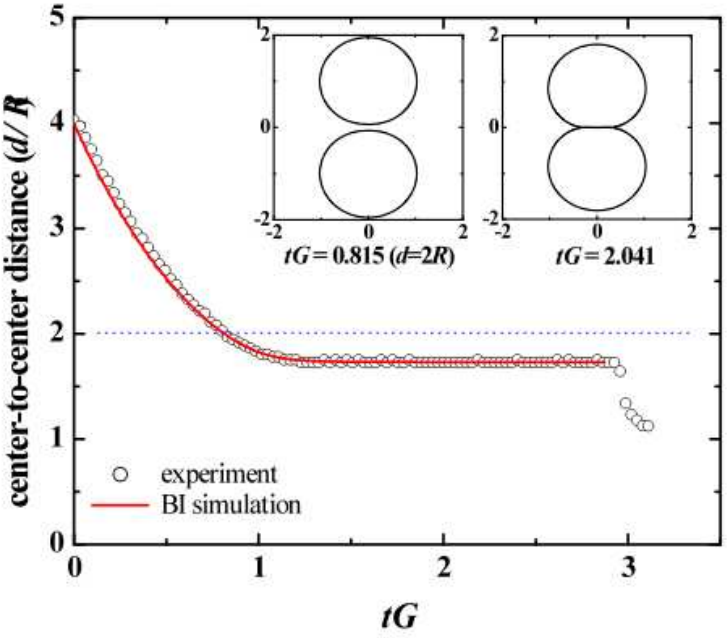

Figure 4: Comparison of experimentally measured center-to-center distance (d/R) versus time tG with numerical values from boundary integral simulation. $Ca = 0.0207$, $\lambda = 0.19$.

problems that can be also described as the interaction of a flow (often of a processing nature) and immersed structures which could be solid or fluid, elastic or rigid, and could come in a broad range of length scales, from nano to macro. Aerodynamic design, insect flight, swimming of microorganisms, cardiac fluid dynamics, and processing of polymeric materials are just a few examples.

The Immersed Boundary (IB) Method introduced by Peskin [58] is a versatile tool for simulating flow-structure interaction for a wide range of applications [59]. The method employs a Lagrangian representation of the immersed structures and their interfacial forces and an Eulerian description of the flow variables (velocity and pressure). The Lagrangian description (tracking) of the immersed boundaries, which does not have to conform to the Eulerian grid, provides a vast structure-building capability while the Eulerian flow description permits the use of efficient flow solvers. The power of the IB Method lies in a seamless connection of the two descriptions by the use of two operations: *spreading* (of interfacial forces) and *interpolation* (of velocity at the immersed boundary), both achieved via mollified delta functions.

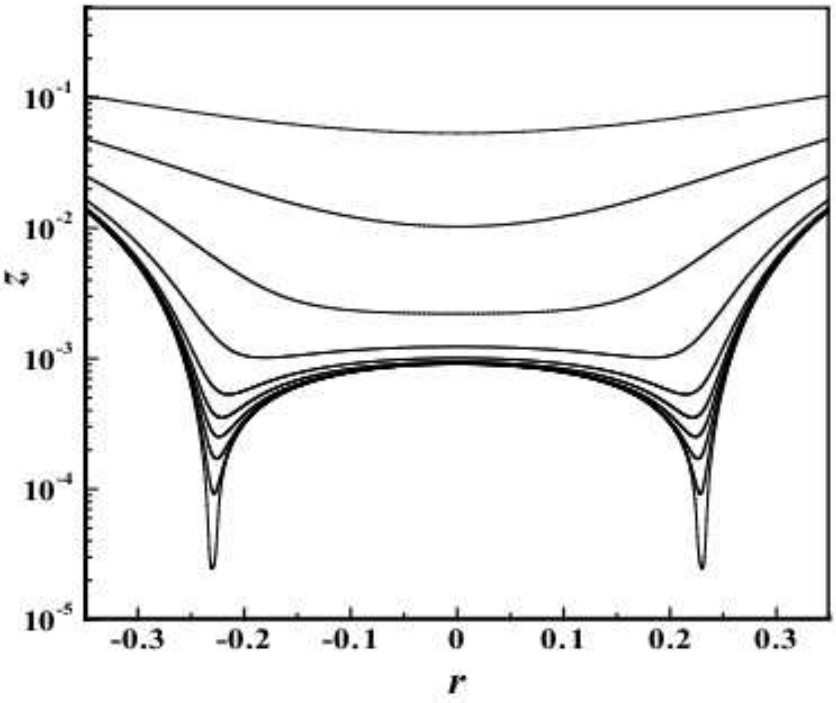

Figure 5: Profile of the thin film gap as it evolves in time (top to bottom). $Ca = 0.0207$, $\lambda = 0.19$.

To describe the method, let us consider an incompressible, Newtonian fluid occupying a domain $\Omega \subset \mathbb{R}^n$, $n = 2, 3$. Inside this domain we assume that there is an immersed, neutrally buoyant, elastic structure (also referred to as boundary or interface). This fluid-immersed interface is composed of a system Γ of elastic fibers whose position at any time t is represented in Lagrangian form by $\mathbf{X}(s,t)$, where $s \in B$ is a Lagrangian parameter. The interface Γ need not be closed or even continuous. The governing equations are:

$$\rho\left(\frac{\partial \mathbf{u}}{\partial t} + \mathbf{u}\cdot\nabla\mathbf{u}\right) = -\nabla p + \mu\nabla^2\mathbf{u} + \mathbf{f}, \tag{33}$$

$$\nabla\cdot\mathbf{u} = 0, \tag{34}$$

$$\frac{\partial \mathbf{X}}{\partial t} = \mathbf{u}(\mathbf{X},t), \tag{35}$$

where ρ and μ are the density and viscosity, respectively (both assumed to be constant in the original formulation of the method). Here $\mathbf{u}(\mathbf{x},t)$ and $p(\mathbf{x},t)$ are the velocity field and the pressure, respectively, described in terms of the Eulerian, Cartesian coordinate $\mathbf{x}$. The term $\mathbf{f}$ represents the singularly

supported interfacial (tension) force of the immersed structure acting onto the fluid. The system (33)-(35) is supplemented with initial and boundary conditions. For concreteness in this discussion, let us assume periodic boundary conditions and that Ω is a rectangular domain in the plane.

The seamless connection of the Lagrangian representation of the immersed structure with the Eulerian representation of the flow is achieved via the identities:

$$\frac{\partial \mathbf{X}}{\partial t} = \int_{\Omega} \mathbf{u}(\mathbf{x}, t)\delta(\mathbf{x} - \mathbf{X}(s, t))d\mathbf{x}, \tag{36}$$

$$\mathbf{f}(\mathbf{x}, t) = \int_{B} \mathbf{F}(\mathbf{X}(\cdot, \cdot), s, t)\delta(\mathbf{x} - \mathbf{X}(s, t))ds, \tag{37}$$

where δ denotes the Dirac delta distribution. In the IB Method, δ is replaced by $\delta_h(\mathbf{x}) = d_h(x)d_h(y)$ and d_h is an approximation of the one-dimensional delta which has a support of $O(h)$. Thus, interfacial forces are actually spread onto the fluid domain via the discrete version of (37). In (37), $\mathbf{F}$ represents the elastic force density of Γ and is described in Lagrangian coordinates. It is typically a nonlinear function of the interfacial configuration, $\mathbf{F} = \mathcal{A}(\mathbf{X})$. For example, if the tangent direction $\mathbf{t}$ along the fibers varies smoothly and if the local elastic energy density is assumed to depend only on the tangential strain $|\frac{\partial \mathbf{X}}{\partial s}|$ then

$$\mathbf{F}(\mathbf{X}, s, t) = \frac{\partial}{\partial s}\left(T\left(\left|\frac{\partial \mathbf{X}}{\partial s}\right|\right)\mathbf{t}\right), \tag{38}$$

where $T(|\frac{\partial \mathbf{X}}{\partial s}|)$ is the fiber (interfacial) tension. In particular, if T is constant, we obtain the uniform surface tension force of a clean (surfactant-free) fluid interface.

In a large number of applications, the structures (immersed boundaries) are very stiff and strong *tangential* forces on these interfaces induce severe time-step restrictions for explicit discretizations [73, 72]. Fully implicit methods and some suitable semi-implicit schemes remove this hindering constraint but seemingly at a cost that renders these options impractical [80, 54]. Recently, there has been some progress towards obtaining robust and practical semi-implicit methods in 2D [55, 44, 43, 15] but the corresponding 3D problem remains largely unsolved.

The IB approach can also be used in the case of variable material properties, i.e. for multi-phase flows by endowing it with a procedure to update ρ and μ in time. This is however a nontrivial problem as these material properties might have large (several orders of magnitude) discontinuity jumps (e.g. air-water) across fluid interfaces. Since the material properties are constant in each of the bulk phases and the interface motion is limited by the CFL condition to less than a mesh size in each time step, it is computationally appealing to update these quantities only in a vicinity of the fluid interface.

Several approaches have been proposed in the literature to address this problem. In tracking methods, the simplest procedure would be to sweep the discrete interface element-wise and identify on which side of each element (line segment) the Eulerian grid points next to it appear. However, this

straightforward *local* procedure [81] yields incorrect results when two interfaces or two disparate segments of the same interface lie too close to each other [82, 79]. To prevent this problem, a more *global* approach, where the whole interface is examined for each Eulerian grid point, must be used. Unverdi and Tryggvason [82] proposed a fluid indicator of this type which is built as the solution of a Poisson equation. This equation incorporates the global properties of the interface and can be fast and efficiently solved for typical rectangular domains. However, it must be solved on the entire computational domain and does not take advantage of the fact that the material quantities only change in a vicinity of the interface. Moreover, as reported in [79], this procedure produces oscillations near the fluid interface and inaccuracies away from it.

In the Level Set Method approach [57], the interface is implicitly given by the zero level set of a function ϕ initialized as the signed distance to the fluid interface. Unlike the material properties themselves, ϕ is continuous and can thus furnish a natural fluid indicator for multi-phase incompressible flows. Moreover, ϕ can be evolved easily via a simple advection equation. Inspired by this observation, a hybrid Level Set-Front Tracking (LeFT) approach was first proposed in [14]. In this hybrid setting, the IB Method equations are supplemented by the level set equation

$$\frac{\partial \phi}{\partial t} + \mathbf{u} \cdot \nabla \phi = 0, \tag{39}$$

and the momentum equation changes to

$$\rho(\phi) \left(\frac{\partial \mathbf{u}}{\partial t} + \mathbf{u} \cdot \nabla \mathbf{u} \right) = -\nabla p + \nabla \cdot \mu(\phi) \left[\nabla \mathbf{u} + \nabla \mathbf{u}^T \right] + \rho(\phi) \mathbf{g} + \mathbf{f}. \tag{40}$$

Note that the interfacial force $\mathbf{f}$ is obtained from the explicit Lagrangian representation of the immersed boundary $\mathbf{X}(\alpha, t)$ using (37) and the interfacial configuration is evolved employing (36). Thus, in this hybrid formulation, the level set function is solely used as a fluid indicator. Given ϕ, the material quantities are obtained by the relations

$$\rho(\phi) = \rho_1 + (\rho_2 - \rho_1) H(\phi), \tag{41}$$

$$\mu(\phi) = \mu_1 + (\mu_2 - \mu_1) H(\phi), \tag{42}$$

where ρ_1, ρ_2 and μ_1, μ_2 are the constant densities and viscosities, respectively and $H(\phi)$ is the Heaviside function defined by

$$H(\phi) = \begin{cases} 0 & \text{if } \phi < 0, \\ 1 & \text{if } \phi \geq 0. \end{cases} \tag{43}$$

Updating ϕ through (39), as it is usually done, quickly leads to a loss of the distance function property of ϕ ($|\nabla \phi| = 1$) due to flow distortion and a re-initialization or re-distancing procedure [76], in which an auxiliary PDE is solved to try to restore ϕ, has to be employed. Moreover, the evolution equation (39) is

solved in the entire computational domain and the local nature of its variation is usually not exploited. An alternative, computationally optimal scheme to compute ϕ was proposed in [21]. The central idea is to employ a fast algorithm (Closest Point Transform, CPT) from *Computational Geometry* [53]. This geometric approach replaces the standard procedures for updating the level set function with an efficient strategy to obtain the signed distance function locally, at optimal cost, and at machine precision for a piece-wise linear representation of the fluid interface.

There has been a recent trend to develop hybrid approaches in an attempt to overcome some of the inherent limitations of traditional tracking and capturing methodologies [60, 75, 14, 32, 29, 21, 89]. The hybrid level-set/front-tracking approach is a particular example of such hybrid strategies that seek to exploit the best features of two different approaches by merging them into one method.

3.1 Adaption

Due to the multi-component nature of the flow, the fluid interfaces are subjected to surface tension which plays a fundamental role in nearly all multi-phase flows of physical interest. The presence of a fluid interface acting with a singular force leads to large gradients localized in a vicinity of the free boundary. Moreover, surface tension can induce the production of focused centers of vorticity and to other small scale phenomena whose adequate capturing often demands computationally prohibitive fine resolutions to uniform grid approaches. This problem can be overcome with a judicious use of a *local mesh refinement technique*.

In the context of the IB and IB-based methods spatial adaption has been incorporated in the form of adaptive mesh refinements (AMR) by Roma, Peskin, and Berger [68] and more recently by Griffith, Hornung, McQueen, and C. S. Peskin [37] and by Ceniceros, Roma, da Silveira-Neto, and Villar [22]. This approach employs the hierarchical grid structure proposed by Berger and Colella [12]. Regions of the flow bearing special interest (such as neighborhoods of a fluid interface, regions of high vorticity, etc.) are covered by block-structured grids, defined as a hierarchical sequence of nested, progressively finer levels (*composite grids*). Each level is formed by a set of disjoint rectangular grids and the refinement ratio between two successive refinement levels are constant and equal to two. Ghost cells are employed around each grid, for all the levels, and underneath fine grid patches to formally prevent the finite difference operators from being redefined at grid borders and at interior regions which are covered by finer levels. Values defined in these cells are obtained from interpolation schemes, usually with second or third order accuracy, and not from solving the equations of the problem. The description of composite grids is given in greater details in [12].

There are three main steps in the AMR approach. *Flagging*: a decision is made to mark a particular set of cells whose collection gives the region where refinement is to be applied. *Grid generation*: grids in each level are generated according to the flagged cells by applying the algorithm for point clusterig due to

Berger and Rigoutsos [51]. *Multi-level solves*: effective iterative methods to solve the linear systems that arise in the projection method on the composite grid need to be employed. Multi-level multigrid methods are typically the natural choices and these can be implemented on a level-by-level basis.

3.2 RT instability in viscous flow

As we have seen, for inviscid 2D flows at small to moderate Atwood numbers, the interface develops thin fluid fingers that subsequently roll-up and appear to eventually collapse with the adjacent fluid interface giving rise to a topological singularity [16]. A relevant question is how small but finite viscosity would affect such a singular event. Recently, a first examination of the problem has been presented in [22] with the use of an AMR-based LeFT method. The setup in [22] is same as that in the aforementioned inviscid case with the exception of nonzero (10^{-4}, cgs units) matched viscosities. Specifically, $A = -0.1$, $\tau = 0.005$, and $g = 10$. The computational domain is the rectangle $\Omega = [0, 1] \times [-1.5, 1.5]$, the velocity satisfies the homogeneous Dirichlet condition at the north and at the south borders, and periodic condition in the horizontal direction.

Snapshots of the interfacial profile during the late stages of the motion are presented in Fig. 6. While there is a similar dynamics to that in the invisicid case there are also notable differences in the fine structure of the fluid fingers (c.f. Fig. 2). There are traces of capillary waves emanating from the fingers as in the inviscid counterpart but the interface motion in the viscous flow is much more complex and the fingers undergo a more pronounced deformation and a stretching leading up to a formation of thin, filament-like structures ($t = 2.28$). The close proximity of interfacial segments suggests a possible pinch-off scenario as that in the inviscid case [16]. However, a close look at the time behavior of the minimum distance between adjacent, opposite interfacial segments, Fig. 7, reveals a contrasting outcome. Slightly before $t = 2.26$, the decrease of the minimum distance saturates, as clearly indicated by the two highest adaptive resolutions, $32 \times 64\,\mathrm{L6}$ and $32 \times 64\,\mathrm{L7}$, equivalent to uniform grid resolutions of 1024×2048 and 2048×4096, respectively. This behavior is reminiscent of the near pinching roll-up observed in a 2D viscous interface undergoing Kelvin-Helmholtz instability where viscous effects appear to prevent finite-time pinching [20, 43]. For the unstably stratified flow, the effects of a viscosity stratification (whether or not this might induce pinch-off) remain to be investigated.

4 Concluding Remarks

As the examples presented here illustrate, the accurate capturing of topologically singular or near singular events in the dynamics of fluid interfaces is a challenging problem. But the investigation of these striking events could help to elucidate fundamental phenomena in interfacial rheology as well as to provide an examination of the range of validity of the underlying models.

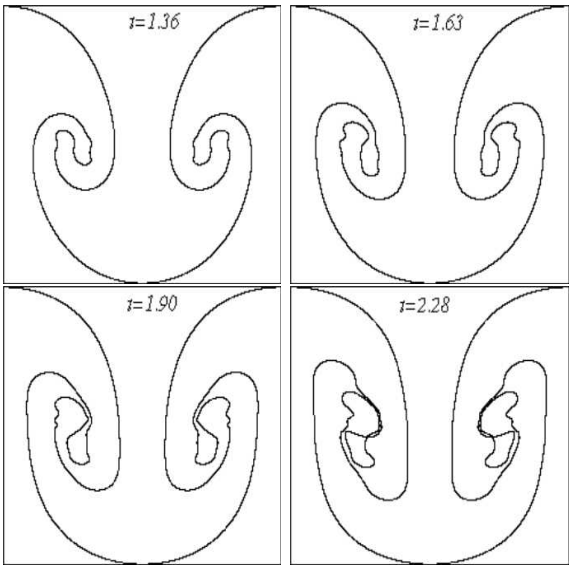

Figure 6: Unstably stratified *viscous* flow: $A = -0.1$ and $\tau = 0.005$, $\mu = 10^{-4}$. Interfacial profiles.

Topological singularities are not to be taken for granted; they constitute a complex process which is very much flow-dependent and largely not well-understood. The numerical investigation of this type of interfacial problems demands a judicious selection of accurate numerical approaches to ensure that these extremely important singular events are not induced numerically.

We have focused here on 2D problems and on front-tracking methodology based on boundary integral and immersed boundary approaches. More effort is needed to develop the corresponding methodologies in 3D to the level that is required for investigating the small scale details of singular events such as flow-induced coalescence or drop break-up. A strong synergy among theory, experiments, and numerical simulations seems indispensable for the investigation of these important processes. In particular, one could check the accuracy of the theory by comparing experimental results with numerical predictions and as a result improve the models to more faithfully capture the underlying physics. In particular, the numerical investigation of topologically singular problems with models that take into account molecular force interactions coupled to the (macro) flow and that more accurately describe the de facto varying material properties in the vicinity of a fluid interface as well as non-uniform surface tension due to surfactants remains an open and challenging field, particularly in 3D.

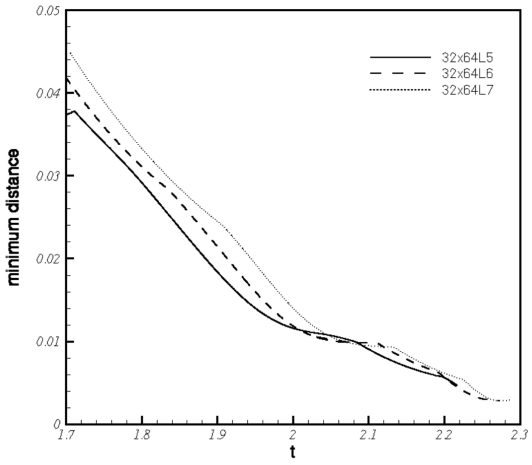

Figure 7: Evolution of the minimum distance from disparate interface segments.

Acknowledgments

The author gratefully acknowledges support by the National Science Foundation under Grant # DMS 0609996.

References

[1] A. Acrivos. The breakup of small drops and bubbles in shear flows. *Ann. N.Y. Acad. Sci.*, 404:1–11, 1983.

[2] A. Acrivos. The deformation of small viscous drops and bubbles in shear flows. *Annu. Rev. Fluid Mech.*, 16:45–66, 1984.

[3] D. M. Anderson, G. B. McFadden, and A. A. Wheeler. Diffuse-interface methods in fluid mechanics. *Annu. Rev. Fluid Mech.*, 30:139, 1998.

[4] U. M. Ascher, S. J. Ruuth, and B. Wetton. Implicit-Explicit Methods for Partial Differential Equations. *SIAM J. Numer. Anal.*, 32(3):797–823, 1995.

[5] S. M. Asida, E. Livne, J. Stein, and L. Metzker. 3-D simulations of Rayleigh-Taylor instability using "VULCAN/3D". *Astrophysics and Space Science*, 298:363–367, 2005.

[6] V. E. Badalassi, H. D. Ceniceros, and S. Banerjee. Computation of multiphase systems with phase field models. *J. Comput. Phys.*, 190:371–397, 2003.

[7] G. R. Baker, D. I. Meiron, and S. A. Orszag. Vortex simulations of the Rayleigh-Taylor instability. *Phys. Fluids*, 23:1485–1490, 1980.

[8] G. R. Baker, D. I. Meiron, and S. A. Orszag. Generalized vortex methods for free-surface flow problems. *J. Fluid Mech.*, 123:477–501, 1982.

[9] G. R. Baker, D. I. Meiron, and S. A. Orszag. Boundary integral methods for axisymmetric and three dimensional Rayleigh-Taylor instability problems. *Physica D*, 12:19–31, 1984.

[10] J. T. Beale, T. Y. Hou, and J. S. Lowengrub. Convergence of a boundary integral method for water waves. *SIAM J. Numer. Anal.*, 33(5):1797–1843, 1996.

[11] J. B. Bell and D. L. Marcus. A second-order projection method for variable density flows. *J. Comput. Phys.*, 101:334–348, 1992.

[12] Berger, M.J. & Colella, P. Local adaptive mesh refinement for shock hydrodynamics. *J. Comput. Phys.*, 82:64–84, 1989.

[13] F. Boyer. A theoretical and numerical model for the study of incompressible mixture flows. *Computer & Fluids*, 31(1):41, 2002.

[14] H. D. Ceniceros. The effect of surfactants on the formation and evolution of capillary waves. *Phys. Fluids*, 15(1):245–256, 2003.

[15] H. D. Ceniceros, J. E. Fisher, and A. M. Roma. Efficient solutions to robust, semi-implicit discretizations of the Immersed Boundary Method. Submitted, 2008.

[16] H. D. Ceniceros and T. Y. Hou. Convergence of a non-stiff boundary integral method for interfacial flows with surface tension. *Math. Comput.*, 67:137–182, 1998.

[17] H. D. Ceniceros and T. Y. Hou. Dynamic generation of capillary waves. *Phys. Fluids*, 11(5):1042–1050, 1999.

[18] H. D. Ceniceros, T. Y. Hou, and H. Si. Numerical study of Hele-Shaw flow with suction. *Phys. Fluids*, 11(9):2471–2486, 1999.

[19] H. D. Ceniceros, A. Karniala, and M. Nitsche. High order quadratures for the evaluation of interfacial velocities in axi-symmetric Stokes flows. Submitted, 2009.

[20] H. D. Ceniceros and A. M. Roma. Study of long-time dynamics of a viscous vortex sheet with a fully adaptive non-stiff method. *Phys. Fluids*, 16:4285–4318, 2004.

[21] H. D. Ceniceros and A. M. Roma. A multi-phase flow method with a fast, geometry-based fluid indicator. *J. Comput. Phys.*, 205:391–400, 2005.

[22] H. D. Ceniceros, A. M. Roma, A. da Silveira-Neto, and M. M. Villar. A robust, fully adaptive hybrid level-set/front-tracking method for two-phase flows with an accurate surface tension computation. Submitted, 2009.

[23] H. D. Ceniceros and J. M. Villalobos. Topological reconfiguration in expanding Hele-Shaw flow. *J. Turbulence*, 3:037, 2002.

[24] Y. C. Chang, T. Y. Hou, B. Merriman, and S. Osher. A level set formulation of Eulerian interface capturing methods for incompressible fluid flows. *J. Comput. Phys.*, 124:449–464, 1996.

[25] R. Chella and V. Viñals. Mixing of a two-phase fluid by a cavity flow. *Phys. Rev. E*, 53:3832, 1996.

[26] V. Cristini, J. Blawzdziewich, and M. Loewenberg. Drop breakup in three-dimensional viscous flows. *Phys. Fluids*, 10:1781–1783, 1998.

[27] B. J. Daly. Numerical study of two fluid Rayleigh-Taylor instability. *Phys. Fluids*, 10(2):297–307, 1967.

[28] R. H. Davis. Buoyancy-driven viscous interaction of a rising drop with a smaller trailing drop. *Phys. Fluids*, 11(5):1016–1028, 1999.

[29] F. S. de Sousa, N. Mangiavacchi, L. G. Nonato, A. Castelo, M. F. Tomé, V. G. Ferreira, J. A. Cuminato, and S. Mckee. A front-tracking/front-capturing method for the simulation of 3D multi-fluid flows with free surfaces. *J. Comput. Phys.*, 198:469–499, 2004.

[30] J. W. Dold. An efficient surface-integral algorithm applied to unsteady gravity waves. *J. Comput. Phys.*, 103:90–115, 1992.

[31] P. G. Drazin and W. H. Reid. *Hydrodynamic stability.* Cambridge monographs on mechanics and applied mathematics. Cambridge University Press, New York, 1981.

[32] S. Manservisi E. Aulisa and R. Scardovelli. A mixed markers and volume-of-fluid method for the reconstruction and advection of interfaces in two-phase and free-boundary flows. *J. Comput. Phys.*, 188:611–639, 2003.

[33] A. Elgowany and N. Ashgriz. Rayleigh-Taylor instability of viscous fluid layers. *Phys. Fluids*, 9(6):1635–1649, 1997.

[34] J. Glimm, J. Grove, X.-L. Li, and D. C. Tan. Robust computational algorithms for dynamic interface tracking in three dimensions. *SIAM J. Sci. Comput.*, 21(6):2240–2256, 2000.

[35] J. Glimm, J. W. Grove, X.L. Li, W. Oh, and D. H. Sharp. A critical analysis of Rayleigh-Taylor growth rates. *J. Comput. Phys.*, 169:652–677, 2001.

[36] J. Glimm, J.W Grove, X.-L. Li, K. M Shyue, Y.N Zeng, and Q. Zhang. Three-dimensional front tracking. *SIAM J. Sci. Comput.*, 19(3):703–727, 1998.

[37] B. E. Griffith, R. D. Hornung, D. M. McQueen, and C. S. Peskin. An adaptive, formally second order accurate version of the immersed boundary method. *J. Comput. Phys.*, 223:10–49, 2007.

[38] F. H. Harlow and J. E. Welch. Numerical calculation of time-dependent viscous incompressible flow of fluid with a free surface. *Phys. Fluids*, 8:2182–2189, 1965.

[39] X. He, R. Zhang, S. Chen, and G. D. Doolen. On the three-dimensional Rayleigh-Taylor instability. *Phys. Fluids*, 11(5):1143–1152, 1999.

[40] M. Horikoshi and K. Nishihara. Vortex generation and deformation of the interface in three-dimensional Rayleigh-Taylor instability. *J. Phys. IV France*, 133:209–212, 2006.

[41] T. Y. Hou, J. S. Lowengrub, and M. J. Shelley. Removing the stiffness from interfacial flows with surface tension. *J. Comput. Phys.*, 114:312–338, 1994.

[42] T. Y. Hou, J. S. Lowengrub, and M. J. Shelley. The long-time motion of vortex sheets with surface tension. *Phys. Fluids*, 9(7):1933–1954, 1997.

[43] T. Y. Hou and Z. Shi. An efficient semi-implicit immersed boundary method for the Navier-Stokes equations. *J. Comput. Phys.*, 227:8968–8991, 2008.

[44] T. Y. Hou and Z. Shi. Removing the stiffness of elastic force from the immersed boundary method for 2D Stokes equations. *J. Comput. Phys.*, 227:9138–9169, 2008.

[45] D. Jacqmin. Calculation of two-phase Navier-Stokes flows using phase-field modeling. *J. Comput. Phys.*, 155:96–127, 1999.

[46] J. Kim, K. Kang, and J. Lowengrub. Conservative multigrid methods for Cahn-Hilliard fluids. *J. Comput. Phys.*, 193:511–543, 2004.

[47] L.G. Leal. Flow-induced coalescence of drops in a viscous fluid. *Phys. Fluids*, 16:1833–1851, 2004.

[48] A. L. F. Lima, A. Silveira-Neto, and J. J. R. Damasceno. Numerical simulation of two-dimensional flows over a circular cylinder using the immersed boundary method. *J. Comput. Phys.*, 189:351–370, 2003.

[49] M. Loewenberg and E. J. Hinch. Numerical simulation of a concentrated emulsion in shear flow. *J. Fluid Mech.*, 321:395–419, 1996.

[50] M. S. Longuet-Higgins and E. D. Cokelet. The deformation of steep surface waves on water I. A numerical method of computation. *Proc. R. Soc. Lond. A.*, 350:1–26, 1976.

[51] M. J. Berger and I. Rigoutsos. An algorithm for point clustering and grid generation. *IEEE Transactions on Systems, Man, and Cybernetics*, 21(5):1278–1286, September/October 1991.

[52] M. Manga and H.A. Stone. Buoyancy-driven interactions between deformable drops at low reynolds numbers. *J. Fluid Mech.*, 256:647–683, 1993.

[53] Mauch, S. *Efficient Algorithms for Solving Static Hamilton-Jacobi Equations*. PhD thesis, California Institute of Technology, 2003.

[54] A. A. Mayo and C. S. Peskin. An implicit numerical method for fluid dynamics problems with immersed elastic boundaries. In A. Y. Cheer and C. P. Van Dam, editors, *Fluid Dynamics in Biology: Proceedings of the AMS-IMS-SIAM Joint Summer Research Conference on Biofluiddynamics*, pages 261–277. American Mathematical Society, 1993.

[55] Y. Mori and C. S. Peskin. Implicit second-order immersed boundary methods with boundary mass. *Comput. Methods Appl. Mech. Engrg.*, 197:2049–2067, 2008.

[56] M. R. Nobari, Y.-J. Jan, and G. Tryggvason. Head-n collision of drops–A numerical investigation. *Phys. Fluids*, 8(1):29–42, 1996.

[57] S. Osher and J. A. Sethian. Fronts propagating with curvature dependent speed: Algorithms based on Hamilton-Jacobi formulations. *J. Comput. Phys.*, 79:12–49, 1988.

[58] C. S. Peskin. Numerical analysis of blood flow in the heart. *J. Comput. Phys*, 25:220–252, 1977.

[59] C. S. Peskin. The immersed boundary method. *Acta Numerica*, pages 477–517, 2002.

[60] S. Popinet and S. Zaleski. A front-tracking algorithm for accurate representation of surface tension. *Int. J. Numer. Meth. Fluids*, 30:775–793, 1999.

[61] C. Pozrikidis. *Boundary Integral and Singularity Methods for Linearized Viscous Flow*. Cambridge Univ. Press, Cambridge, U.K., 1992.

[62] C. Pozrikidis. Interfacial dynamics for Stokes flows. *J. Comput. Phys.*, 169(2):250, 2001.

[63] E. G. Puckett, A. S. Almgren, J. B. Bell, D. L. Marcus, and W. J. Rider. A high order projection method for tracking fluid interfaces in variable density incompressible flows. *J. Comput. Phys.*, 100:269–282, 1997.

[64] D. I. Pullin. Numerical studies of surface-tension effects in nonlinear Kelvin-Helmholtz and Rayleigh-Taylor instability. *J. Fluid Mech.*, 119:507–532, 1982.

[65] Lord Rayleigh. Investigation of the character of equilibrium of an incompressible heavy fluid of variable density. *Proceedings of the London Mathematical Society*, 14:170–177, 1883.

[66] W. J. Rider and D. B. Kothe. Reconstructing volume tracking. *J. Comput. Phys.*, 141:112, 1998.

[67] A. J. Roberts. A stable and accurate numerical method to calculate the motion of a sharp interface between fluids. *IMA J. Appl. Math.*, 31:13–35, 1983.

[68] A. M. Roma, C. S. Peskin, and M. J. Berger. An adaptive version of the immersed boundary method. *J. Comput. Phys.*, 153:509–534, 1999.

[69] R. Scardovelli and S. Zaleski. Direct numerical simulation of free-surface and interfacial flow. *Annu. Rev. Fluid Mech.*, 31:567–603, 1999.

[70] M. J. Shelley. A study of singularity formation in vortex sheet motion by a spectrally accurate vortex method. *J. Fluid Mech.*, 244:493–526, 1992.

[71] A. Sidi and M. Israeli. Quadrature methods for periodic singular and weakly singular Fredholm integral equations. *J. Sci. Comput.*, pages 67–91, 1988.

[72] J. M. Stockie and B. R. Wetton. Analysis of stiffness in the immersed boundary method and implications for time-stepping schemes. *J. Comput. Phys.*, 154:41–64, 1999.

[73] J. M. Stockie and B. T. R. Wetton. Stability analysis for the immersed fiber problem. *SIAM J. Appl. Math*, 55(6):1577–1591, 1995.

[74] H.A. Stone and L. G. Leal. Relaxation and breakup of an initially extended drop in an otherwise quiescent fluid. *J. Fluid Mech.*, 198:399–427, 1989.

[75] M. Sussman and E. G. Puckett. A coupled level set and volume-of-fluid method for computing 3d and axisymmetric incompressible two-phase flows. *J. Comput. Phys.*, 162:301–337, 2000.

[76] M. Sussman, P. Smereka, and S. Osher. A level set approach for computing solutions to incompressible two-phase flow. *J. Comput. Phys.*, 114:146–159, 1994.

[77] G. I. Taylor. The instability of liquid surfaces when accelerated in a direction perpendicular to their planes. *Proceedings of the Royal Society of London, Series A, Mathematical and Physical Sciences*, 201:192–196, 1950.

[78] G. Tryggvason. Numerical simulations of the Rayleigh-Taylor instability. *J. Comput. Phys.*, 75:253–282, 1988.

[79] G. Tryggvason, B. Bunner, A. Esmaeeli, D. Juric, N. Al-Rawahi, W. Tauber, J. Han, S. Nas, and Y.-J. Jan. A front-tracking method for computations of multiphase flow. *J. Comput. Phys.*, 169:708–759, 2001.

[80] C. Tu and C. S. Peskin. Stability and instability in the computations of flows with moving immersed boundaries: a comparison of three methods. *SIAM J. Sci. Stat. Comput.*, 13(6):1361–1376, 1992.

[81] H. S. Udaykumar, H.-C. Kan, W. Shyy, and R. Tran-Son-Tay. Multiphase dynamics in arbitrary geometries on fixed cartesian grids. *J. Comput. Phys.*, 137:366–405, 1997.

[82] S. O. Unverdi and G. Tryggvason. A front-tracking method for viscous, incompressible, multifluid flows. *J. Comput. Phys.*, 100:25–37, 1992.

[83] J. T. Waddell, C. E. Niederhaus, and J. W. Jacobs. Experimental study of Rayleigh-Taylor instability: low Atwood number liquid systems with single-mode initial perturbations. *Phys. Fluids*, 13(5):1263–1273, 2001.

[84] S. V. Weber, G. Dimonte, and M. M. Marinak. Arbitrary Lagrange-Eulerian code simulations of turbulent Rayleigh-Taylor instability in two and three dimensions. *Laser and Particle Beams*, 21:455–461, 2003.

[85] Y. Yoon, F. Baldessari, H. D. Ceniceros, and L. G. Leal. Coalescence of two equally-sized deformable drops in an axisymmetric flow. *Phys. Fluids*, 19:102102, 2007.

[86] Y. Yoon, A. Hsu, and L.G. Leal. Experimental investigation of the effects of copolymer surfactants in flow-induced coalescence of drops. *Phys. Fluids*, 19:023102, 2007.

[87] G. K. Youngren and A. Acrivos. On the shape of a gas bubble in a viscous extensional flow. *J. Fluid Mech.*, 76:433, 1976.

[88] P. Yue, J. J. Feng, C. Liu, and J. Shen. A diffuse-interface method for simulating two-phase flows of complex fluids. *J. Fluid Mech.*, 515:293–317, 2004.

[89] X. Zheng, J. Lowengrub, A. Anderson, and V. Cristini. Adaptive unstructure volume remeshing-II: Application to two- and three-dimensional level-set simulations of multiphase flow. *J. Comput. Phys.*, 208:626–650, 2005.

[90] A. Z. Zhinchenko and R. H. Davis. Large-scale simulations of concentrated emulsion flows. *Phil. Trans. R. Soc. Lond. A*, 361:813–845, 2003.

[91] A. Z. Zinchenko, M. A. Rother, and R. H. Davis. A novel boundary integral algorithm for viscous interaction of deformable drops. *Phys. Fluids*, 9:1493–1511, 1997.